In Vivo Protein Synthesis Rate Determination in Primary or Recurrent Brain Tumors Using L-[1-^{11}C]-Tyrosine and PET

A.T.M. Willemsen, A. van Waarde, A.M.J. Paans, J. Pruim, G. Luurtsema, K.G. Go and W. Vaalburg

PET-Center and Department of Neurosurgery, University Hospital Groningen, Groningen, The Netherlands

The applicability of protein synthesis rate (PSR) determination with L-[1-^{11}C]tyrosine (^{11}C-TYR) and PET was assessed in patients suspected of a primary or recurrent brain tumor. **Methods:** Simultaneous to intravenous injection of 265 MBq of ^{11}C-TYR, dynamic PET acquisition was started and continued for 50 min. Arterial samples were taken and analyzed for ^{11}C-TYR and metabolites. Based on this data, a model was proposed and the corresponding PSR calculated. **Results:** Plasma metabolites were $^{11}CO_2$, ^{11}C-proteins and ^{11}C-L-DOPA, constituting more than 50% of total plasma radioactivity at 40 min postinjection. Plasma $^{11}CO_2$ reached a plateau of around 25% of total plasma radioactivity at 20 min postinjection. Plasma ^{11}C-protein was not detected before 10 min postinjection, but increased exponentially afterwards to 20% at 40 min postinjection. Plasma ^{11}C-L-DOPA was the only acid-soluble radioactive metabolite detected and was less than 8% at 40 min postinjection. Using a five-compartment model, it was shown that while the net PSR was dependent on the recycling of amino acids from protein, the amino acid incorporation was not, which was thus used for subsequent analysis. It was found that our curve-fitting results were unreliable due to the exchange of ^{11}C-TYR between plasma and erythrocytes whereas the graphical Patlak-Gjedde analysis is hardly influenced by this transport phenomenon. The average amino acid incorporation rate thus calculated was 0.7 nmole/ml·min for nontumor tissue with a tumor versus nontumor average ratio of 1.7. **Conclusion:** The assessment of the PSR with TYR-PET is valuable and relatively simple to implement clinically.

Key Words: L-[1-^{11}C]-tyrosine; protein synthesis rate; positron emission tomography

J Nucl Med 1995; 36:411–419

PET allows the in vivo study of physiological rather than anatomical parameters. Quantification of the regional rate of glucose metabolism, using the tracer 2-[^{18}F]-fluoro-2-deoxy-D-glucose (FDG), has found wide clinical application. Although FDG-PET has been very successful over the years, it is evident that it is not the optimal tracer in all cases. Especially in neuro-oncology, sensitivity and specificity of tumor detection are hampered in regions with a high basal metabolism such as the brain (*1–4*) while gliomas may exhibit both elevated and reduced rates of glucose metabolism. Furthermore, inflammatory cells have been reported to exhibit increased glucose metabolism. (*5–7*).

To circumvent these problems, the in vivo study of other metabolic processes may be fruitful, such as the rates of protein, RNA or DNA synthesis (*8,9*). To determine the protein synthesis rate (PSR), various labeled amino acids have been studied. These include L-[methyl-^{11}C]methionine (*4,10–15*), L-[1-^{11}C]methionine (*16,17*), L-[1-^{11}C]leucine (*18–20*), L-[1-^{11}C] tyrosine (*14,21–24*), ^{11}C-valine (*25,26*), ^{18}F-fluorotyrosine (*27,28*) and ^{14}C- or ^{18}F-labeled phenylalanine (*29,30*). Metabolic pathways of the tracer, kinetic modeling and clinical applicability have all been studied to some extent. In this study, the potential of PSR determination in humans using L-[1-^{11}C]tyrosine (^{11}C-TYR) and PET is reported. The specific goals comprise: identification and quantification of the plasma metabolites of ^{11}C-TYR as a function of time in humans; development and validation of a kinetic model; and the subsequent determination of PSR in tumor and nontumor tissue.

Metabolic Pathways of L-[1-^{11}C]Tyrosine

During a PET study (±60 min), the main metabolic pathway of ^{11}C-TYR in tissue is irreversible to the incorporation of ^{11}C into protein (*31*). Minor metabolic pathways are decarboxylation and synthesis of L-[p-hydroxy]-[1-^{11}C] phenylpyruvic acid, L-[p-hydroxy]-[1-^{11}C]lactic acid and L-[1-^{11}C]DOPA (*31*). Further metabolism results in the release of the label as $^{11}CO_2$. Carbon-11 protein may be found in plasma as it is produced in the liver and released in the circulation. Plasma metabolites in man can be determined in arterial blood samples. For human tissues, however, only the total radioactivity can be directly established from PET data. Therefore, animal experiments are required to assess the metabolites in tissue.

Animal Experiments

Metabolic studies with L-[1-^{14}C]tyrosine as well as PSR determination in rats have been reported (*31*). The meta-

Received Mar. 14, 1994; revision accepted Sept. 20, 1994.

For correspondence or reprints contact: Dr. A.T.M. Willemsen, PET-Center, University Hospital Groningen, P.O. Box 30.001, 9700 RB Groningen, The Netherlands.

bolic studies revealed a significant amount of $^{14}CO_2$ in plasma, although the amount in tissue was negligible. Other labeled nonprotein metabolites in tissue were less than 4% of total tissue activity. Non-protein metabolites in plasma may reach 10% and proteins in plasma reached 85% leaving less than 10% free tyrosine at 60 min. Paans et al. (*32*) established the PSR for rhabdomyosarcoma to be 0.4 ± 0.1 nmole/(g·min) while the faster growing Walker 256 carcinosarcoma gave a PSR of 0.8 ± 0.2 nmole/(g·min).

MATERIALS AND METHODS

Synthesis of L-[1-^{11}C]-Tyrosine

^{11}C-TYR was synthesized via ^{11}C-carboxylation of an α-lithiated isocyanide according to Bolster et al. via robotic synthesis (*16,21*). In brief, p-methoxyphenylethylisocyanide was lithiated and carboxylation was carried out with $^{11}CO_2$. After acid hydrolysis the racemic mixture was pH neutralized and then purified and separated enantiomerically by HPLC. Finally, tyrosine in a 0.9% NaCl solution was passed through a sterile 0.22 μm Millipore filter. Synthesis was remote controlled using a robot system. Total synthesis time was 60 min (EOB), including HPLC purification. Typically, 750–1000 MBq ^{11}C-TYR was produced with a specific activity in excess of 40 GBq/μmol.

Patients

So far, 11 patients participated (6 male, 5 female, age 40 ± 11 yr) in the study. The study was approved by the Hospital Medical Ethics Committee and the patients gave informed consent. All subjects were suspected of a primary or a recurrent brain tumor on the basis of clinical data and CT/MRI, and were scheduled for further treatment. In addition, metabolite data were obtained from seven patients who had static acquisition only.

Data Acquisition

Patients had fasted for at least 6 hr when they were positioned under the PET camera (Siemens ECAT 951/31, FWHM = 6 mm) with low ambient light and noise. Photon attenuation was measured using a retractable ring source filled with ^{68}Ge/^{68}Ga. Carbon-11-TYR (265 ± 115 MBq) was injected intravenously over a 1-min period. Dynamic image acquisition (10 × 30 sec, 3 × 5 min and 3 × 10 min) was started simultaneously with the injection. Arterial plasma samples were obtained every 10 sec for the first minute, then every 30 sec for the next 4 min, and at 10, 15, 20, 30 and 40 min postinjection. All blood samples were centrifuged (2000 g, 5 min) to acquire plasma. Whole-blood radioactivity was also measured for some patients. Typical delays between sampling and centrifugation were three min. Some samples were centrifuged immediately (delay <1 min) to study the exchange of ^{11}C-TYR between plasma and erythrocytes. Plasma samples acquired at 0.5, 1, 2.5, 5, 10, 15, 20, 30 and 40 min were analyzed for $^{11}CO_2$ and ^{11}C-proteins, while samples acquired at 10, 20 or 40 min were analyzed using HPLC as described below.

Metabolite Analysis

All reagents used were of analytical grade. L-Tyrosine, 2-propanol, HCl, NaOH, $NaHCO_3$ and $NaH_2PO_4 \cdot H_2O$ were from Merck (Darmstadt, Germany). L-[3,4-dihydroxy]phenylalanine (L-DOPA), DL-p-hydroxyphenylpyruvic acid and DL-p-hydroxyphenyllactic acid were from Sigma (St. Louis, MO).

Plasma $^{11}CO_2$ was assayed in plasma samples using a modification of the procedure described for ^{11}C-palmitate by Fox et al. (*33*). Duplicate plasma samples (0.5 ml each) were pipetted in 10-ml tubes containing 3 ml 2-propanol and 1 ml 0.09 *M* $NaHCO_3$ (carrier). One sample was acidified by the addition of 1 ml 6 N HCl and the other was alkalinized by the addition of 1 ml 0.1 N NaOH. The tube contents were thoroughly mixed and placed in a ultrasonic bath (Branson 8200, 60°C) for 30 min. Radioactivity was then determined using a gamma counter. The difference between the two samples was considered to represent evaporated $^{11}CO_2$. The procedure was checked using $NaH^{11}CO_3$ and ^{11}C-TYR as internal standards. Under these conditions $^{11}CO_2$ was quantitatively (≥98%) evaporated, whereas ^{11}C-TYR was retained for >99%.

Labeled plasma protein was determined using the method of Ishiwata et al. (*31*). Duplicate plasma samples (0.25 ml) were pipetted into Eppendorf cups. To one sample, 0.5 ml ice-cold 7.5% (w/v) trichloroacetic acid (TCA) was added; the other sample was covered and stored at room temperature. In the acidified sample, protein was precipitated by short centrifugation (2 min, 14,000 g). The pellet was washed three times with 0.5 ml TCA, each followed by centrifugation (2 min, 14,000 g) and removal of the supernatant. Radioactivity in the pellet and in the untreated plasma sample was then determined using the calibrated gamma well counter. Pellet radioactivity (after subtraction of a zero-time blank) was considered to represent incorporation of L-[1-^{11}C]tyrosine into plasma proteins.

Acid-soluble metabolites of ^{11}C-TYR in human plasma were determined using reversed phase HPLC. A plasma sample (0.5 ml) was mixed with 0.25 ml ice-cold 7.5% (w/v) TCA and protein was removed by short centrifugation (2 min, 14,000 g). The supernatant was filtered (0.4 μ), spiked with cold standards (10 μg of L-DOPA, L-tyrosine, p-hydroxy-phenylpyruvic acid and p-hydroxy-phenyllactic acid) and directly injected into the reversed-phase HPLC system (C18). The mobile phase consisted of 0.1 *M* NaH_2PO_4 (room temperature, flow rate 3 ml·min^{-1}). Radioactivity in 0.5–2.5 ml fractions of the eluate was finally determined using the calibrated gamma counter. This resulted in a baseline separation of all compounds of interest. Radioactivity applied to the column was quantitatively recovered in the eluate.

Compartment Model

Based on the above data, a kinetic model for the transport of ^{11}C-TYR and its labeled metabolites is proposed (Fig. 1). It consists of five compartments: (1) free tyrosine in plasma (2) free tyrosine in tissue and (3) protein in tissue, ^{11}C is released as (4) $^{11}CO_2$ with rate constant k_4, which in turn is transported to the plasma (5) with rate constant k_5. Transport of labeled protein into plasma as well as exogenous recycling of amino acids by proteolysis of proteins labeled with ^{11}C-TYR are assumed to be negligible on the time scale of the study. Thus the following equations hold:

$$\frac{dC_e^*}{dt} = k_1^* C_p^* - (k_2^* + k_3^* + k_4^*) C_e^*, \qquad \text{Eq. 1}$$

$$\frac{dC_{pr}^*}{dt} = k_3^* C_e^*, \qquad \text{Eq. 2}$$

$$\frac{dC_m^*}{dt} = k_4^* C_e^* - k_5^* Cm^*, \qquad \text{Eq. 3}$$

with C_p^* the concentration of ^{11}C-TYR in plasma; C_e^* the concentration of ^{11}C-TYR in the precursor pool; C_{pr}^* the concentration of labeled protein in tissue; C_m^* the concentration of $^{11}CO_2$ in tissue;

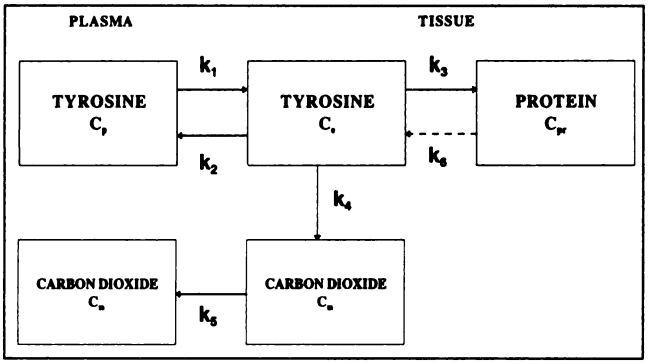

FIGURE 1. Compartmental model of L-[1-^{11}C]tyrosine and ^{11}C-metabolites. The transport of tyrosine between plasma, compartment C_p, and precursor, compartment C_e, is modeled with rate constants k_1 and k_2. The incorporation into protein, compartment C_{pr}, is modeled with rate constant k_3. Recycling of amino acids by the degradation of protein, rate constant k_6, is assumed to be negligible for the labeled but not for the unlabeled protein. The only alternative pathway is decarboxylation which releases the label as carbon dioxide, compartment C_m, with rate constant k_4. $^{11}CO_2$ is then transported to plasma with rate constant k_5.

and k_i^* (i = 1..5) the rate constants. The superscript is used to indicate that the parameter relates to the labeled compound.

From these equations, the relation between measured tissue activity and measured plasma activity as a function of time can be obtained as was shown by Hawkins et al. (*19*). For the unlabeled endogenous proteins, amino acid recycling cannot be ignored. It has been published (*13,25,34,35*) that about 50% of the precursor amino acid pool (C_e) is due to amino acid recycling. Under steady state conditions the net rate of protein synthesis (PSR_n) is then given by:

$$PSR_n = k_3C_e - k_6C_{pr} = \phi k_3C_e, \qquad \text{Eq. 4}$$

with $\phi = 1 - k_6C_{pr}/k_3C_e$ the recycling factor and k_6 the rate constant for the transport of unlabeled protein to unlabeled amino acid due to recycling.

If the primary objective is to study the amino acid incorporation rather than net protein synthesis, one can alternatively take:

$$PSR = k_3C_e. \qquad \text{Eq. 5}$$

The concentration of nonlabeled (endogenous) free tyrosine (C_e) is, under steady state conditions and including the recycling with rate constant k_6, given by:

$$\begin{aligned} k_1C_p &= (k_2 + k_3 + k_4)C_e - k_6C_{pr} \\ &= (k_2 + k_3 + k_4)C_e - (1 - \phi)k_3C_e \\ &= (k_2 + \phi k_3 + k_4)C_e. \end{aligned} \qquad \text{Eq. 6}$$

Following the same method as with the FDG model (*36*), the combination of Equations 4 to 6 yields:

$$\begin{aligned} PSR_n &= \frac{\phi k_1k_3}{k_2 + \phi k_3 + k_4}C_p \\ &= \frac{\phi k_1k_3}{k_2 + k_3 + k_4}\frac{k_2 + k_3 + k_4}{k_2 + \phi k_3 + k_4}C_p = \phi K\varepsilon C_p. \end{aligned} \qquad \text{Eq. 7}$$

$$PSR = \frac{k_1k_3}{k_2 + \phi k_3 + k_4}C_p = K\varepsilon C_p, \qquad \text{Eq. 8}$$

with

$$K = \frac{k_1k_3}{k_2 + k_3 + k_4},$$

and

$$\varepsilon = \frac{k_2 + k_3 + k_4}{k_2 + \phi k_3 + k_4}.$$

Hawkins et al.(*19*) reported rate constants for L-[1-^{11}C]leucine. Assuming their values ($k_2 \cong 0.4$, $k_3 \cong 0.04$, $k_4 \cong 0.1$) to be transferable to our case and with a recycling of 50% ($\phi = 0.5$) (*13,25,34,35*) we find an ε of 1.04. Equation 8 can thus be approximated by:

$$PSR \cong KC_p, \qquad \text{Eq. 9}$$

indicating that the amino acid incorporation rate is not affected by the amino acid recycling. Considering that chemically ^{11}C and ^{12}C are identical, we have $k_i = k_i^*$ (i = 1..5). Consequently the rate constants obtained for labeled tyrosine can be substituted into Equations 7 and 9.

Provided that the protein is effectively trapped in the tissue, the quotient $k_1k_3/(k_2 + k_3 + k_4)$ can also be obtained using a graphical method (*37,38*) as described below. Also, if the various ^{11}C-metabolites in tissue can be ignored, animal experiments showed them to be less than 4% (*31*) then the tissue activity as measured with PET is given by:

$$C_i^* = (1 - V_b)(C_e^* + C_{pr}^* + C_m^*) + V_bC_b^*, \qquad \text{Eq. 10}$$

with V_b the blood volume measured and C_b^* the total blood activity concentration (i.e., including the labeled metabolites).

After the first fast kinetic phase the following relations apply:

$$C_e^* \cong \frac{k_1}{k_2 + k_3 + k_4}C_p^*(t), \qquad \text{Eq. 11}$$

$$C_m^* \cong \frac{k_4}{k_5}C_e^* \cong \frac{k_4}{k_5}\frac{k_1}{k_2 + k_3 + k_4}C_p^*(t), \qquad \text{Eq. 12}$$

$$C_{pr}^* = k_3\int C_e^*(\tau)\,d\tau \cong \frac{k_1k_3}{k_2 + k_3 + k_4}\int C_p^*(\tau)\,d\tau. \qquad \text{Eq. 13}$$

By combining Equations 10 through 13 one obtains:

$$\begin{aligned} \frac{C_i^*}{C_p^*} &= V_b\frac{C_b^*}{C_p^*} + \frac{(1 - V_b)k_1}{k_2 + k_3 + k_4}\left(1 + \frac{k_4}{k_5}\right) \\ &\quad + \frac{(1 - V_b)k_1k_3}{k_2 + k_3 + k_4}\frac{\int C_p^*(\tau)\,d\tau}{C_p^*(t)}, \end{aligned} \qquad \text{Eq. 14}$$

where C_i^*/C_p^* is denoted as the distribution volume and $\int C_p^*(\tau)\,d\tau/C_p^*(t)$ is denoted as the apparent time.

Considering that C_i^* is measured by the PET camera and that C_p^* can be established from arterial blood samples, a graphical display of C_i^*/C_p^* versus $\int C_p^*(\tau)\,d\tau/C_p^*(t)$ can be made. The first term on the right-hand side of equation 14, $V_bC_b^*/C_p^*$, is considered to be a perturbation, but can be ignored for the studies reported here (see

TABLE 1
Plasma Kinetics of L-[1-^{11}C]Tyrosine in Humans as a Percentage of Total Plasma Radioactivity

Time (min)	CO_2	Protein	Acid-soluble metabolites	L-Tyrosine
0.5	1.7 ± 1.2	<1%	<1%	98.3 ± 1.2
1	3.6 ± 1.8	<1%	<1%	96.4 ± 1.8
2.5	8.4 ± 3.0	<1%	<1%	91.6 ± 3.0
5	13.4 ± 5.4	<1%	<1%	86.6 ± 5.4
10	16.8 ± 5.0	<1%	2.5 ± 1.6	80.7 ± 5.2
15	20.8 ± 4.5	<1%	4.2 ± 1.9	75.0 ± 4.9
20	22.4 ± 5.5	1.7 ± 2.3	5.7 ± 2.2	70.2 ± 6.4
30	26.3 ± 5.9	7.0 ± 2.9	7.0 ± 0.9	59.7 ± 6.6
40	24.5 ± 6.1	18.4 ± 4.5	8.4 ± 2.3	48.7 ± 7.9

Data are expressed as mean ± s.d. of up to 18 oncological patients.

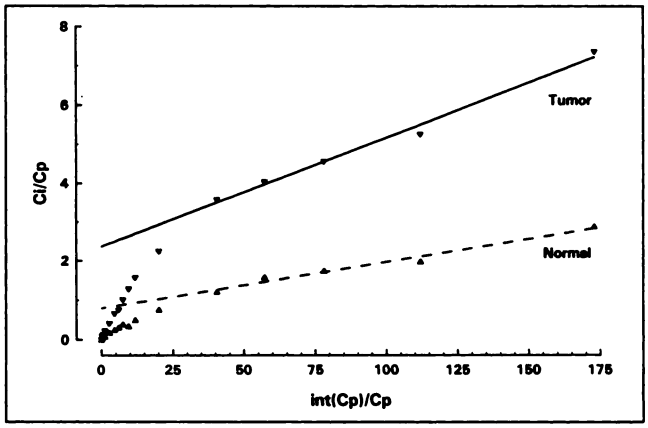

FIGURE 3. Patlak graphical display of a tumor and of the contralateral region with fit.

results). The second term is a constant and does not influence the slope. The third term determines the slope of the resulting curve, $(1 - V_b)K$, from which the amino acid incorporation rate (Eq. 9) can be calculated. So, provided that the blood volume is small ($1 - V_b \cong 1$) it can be concluded that neither the blood volume nor the $^{11}CO_2$ activity in tissue, affect the final result. If the blood volume is not negligible the calculated PSR is influenced by the blood volume fraction which should then be measured separately.

RESULTS

Plasma Metabolite Analysis

Labeled plasma metabolite data as percentage of total plasma radioactivity is summarized in Table 1. Labeled CO_2 is detectable within 1 min whereas proteins and acid-soluble labeled plasma metabolites remain low (<5%) for the first 15 min. Total metabolite fraction reaches 50% of plasma radioactivity at 40 min. The only acid-soluble labeled plasma metabolite identified was ^{11}C-L-DOPA for times up to 40 min postinjection. Total plasma metabolite fraction is given in Figure 2. After the first 5 min the metabolite fraction increases almost linearly with a slope of 1%/min. This allows the estimation of the perturbation in the slope between the distribution volume and the apparent

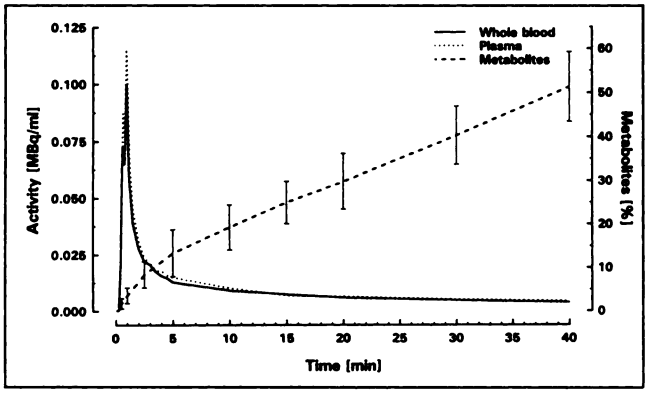

FIGURE 2. Plasma and whole blood activity as a function of time. Data are not corrected for metabolites. The total metabolite fraction as a function of time is also indicated.

time (Eq. 14) resulting from the radioactivity in the measured blood volume. Since the whole blood and the total plasma time-activity data are virtually identical after 5 min (see below), we have:

$$V_b C_b^*/C_p^* \cong V_b(C_p^* + C_{pm}^*)/C_p^* = V_b + V_b C_{pm}^*/C_p^*,$$

with C_{pm}^* the total plasma metabolite activity. The first term, V_b, is constant and therefore does not influence the slope. With a maximum blood volume of 5% for the brain and a plasma metabolite fraction of maximum 50% within the duration of the study we obtain:

$$0 \le V_b C_{pm}^*/C_p^* \le 0.025.$$

As $C_i^*/C_p^* \ge 1$ after the first fast kinetic phase, see Figure 3, the perturbation can easily be ignored.

Plasma, Tissue and Whole Blood Time-Activity Data

Figure 2 shows a typical example of a plasma and whole blood time-activity curve. These virtually identical curves reach their maximum at approximately one minute after which they decrease rapidly. Five to ten minutes later the curves reach a slow kinetic period. The similarity between the whole blood and plasma time-activity curves enables the substitution of the (uncorrected) plasma activity for the whole blood activity in Equation 14 which was used to assess the influence of the blood volume above. As described in the methods section, some samples were separated as quickly as possible. At 1.5 and 2 min a plasma to pellet ratio of up to 3 was found. This ratio decreased rapidly, indicating fast dynamics between plasma and erythrocyte pool, and reaches unity for samples obtained after 5 min.

Typical tissue time-activity curves for a tumor and for the contralateral region are given in Figure 4. Maximum activities are reached within the first 5–10 min after which the measured activity decreases. This loss of activity is caused by the transport of $^{11}CO_2$ from tissue to plasma. The corresponding Patlak curves, however, (Figure 3) rapidly approach a straight line indicating irreversible trapping of ^{11}C in proteins even though the total measure tissue radioactivity decreases.

Modeling

On the basis of the model description and the difficulties in obtaining a correct plasma input function, the graphical Patlak analysis (*37,38*) was considered as the reference

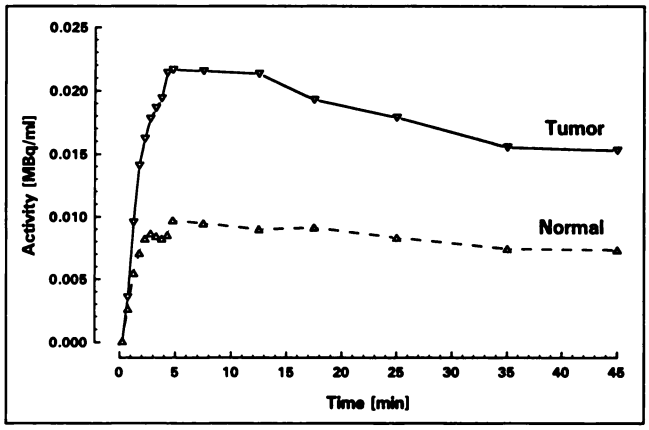

FIGURE 4. Tissue time-activity curves for a tumor region and for the contralateral region. See also Figures 3, 5 and 7.

(see discussion). Also several kinetic models were tested to calculate the PSR by curve fitting. Therefore, the model was written as follows:

$$\dot{X} = AX + BU, \qquad \text{Eq. 15a}$$

$$Y = CX + DU, \qquad \text{Eq. 15b}$$

with $X = [C_e^* C_m^* C_{pr}^*]^T$, $U = [C_p^* C_b^*]^T$ A, B, C, D the state-space matrices and C_b^* the radioactivity of whole blood where superscript T indicates the transpose of the vector and $\dot{X}$ indicates the derivative of X.

By setting the state-space matrices A, B, C and D the model can be simulated and the measured signal (Y) can then be calculated. For the model described above the following matrices are found:

$$A = \begin{bmatrix} -(k_2 + k_3 + k_4) & 0 & 0 \\ k_4 & -k_5 & 0 \\ k_3 & 0 & 0 \end{bmatrix} \quad B = \begin{bmatrix} k_1 & 0 \\ 0 & 0 \\ 0 & 0 \end{bmatrix}$$

$$C = [1 - V_b 1 - V_b 1 - V_b]^T \quad D = [0\ V_b]^T. \qquad \text{Eq. 16}$$

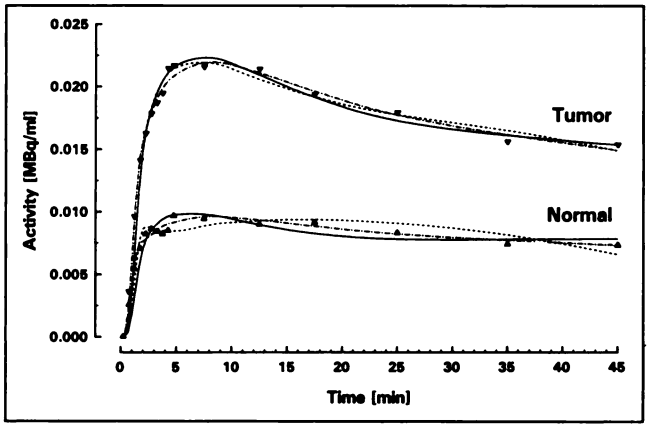

FIGURE 5. Curve fits for the kinetic tyrosine model for tumor and normal tissue. Four different model variants were investigated as described in the text. Solid line: $k_5 = V_b = 0$; Dash-dot line: $k_5 = 0$, $V_b \neq 0$; Medium-dash: $k_5 \neq 0$, $V_b = 0$; Dotted line: $k_5 \neq 0$, $v_b \neq 0$. See also Figures 4 and 5.

In two simpler models either k_5 or V_b was set to zero. Finally a fourth model was selected in which both k_5 and V_b were set to zero. The simulation result was fitted to the measured result by minimizing the (unweighted) χ^2 (Figure 5). The full model with six degrees of freedom had severe difficulties finding the optimal fit and negative k_3 values were obtained on some occasions resulting in a negative PSR. This indicates overdetermination of the system. Removing k_5 these problems were solved although the PSR values found were a factor of 2 lower than those determined with the graphical Patlak analysis. Furthermore, PSR values for normal tissue were now dependent on the area selected. Similar problems occurred with $V_b = 0$ or with $V_b = 0$ and $k_5 = 0$. No model gave identical PSR values as the Patlak reference.

In Vivo PSR Determination

Considering the above, the PSR for the various tumors as well as for the contralateral brain were calculated using the Patlak analysis method. The results are given in Table 2. The average tumor PSR was found to be 1.13 ± 0.59 nmol/ml·min. The contralateral PSR was found to be 0.66 ± 0.39 nmol/ml·min. The ratio tumor to nontumor was found to be 1.72 ± 0.44. The Patlak method was also applied to the data on a pixel by pixel basis. So, for each pixel in the volume a separate independent calculation of the PSR was performed. The result is given in Figure 6 together with the original activity distribution image. Figure 3 shows the corresponding Patlak plots for the tumor and the contralateral region with their fits. As can be noticed the signal to noise ratio in the parametric image is reduced as compared to the activity distribution indicating that the individual voxel values are less reliable. However, the mean pixel PSR value of a region of interest is practically identical to the PSR value as calculated from the corresponding mean time-activity curve. Furthermore, the tumor appears to be smaller and better outlined on the PSR image than on the activity image, although it is too early to speculate on the underlying reasons.

DISCUSSION

The average protein synthesis rate of 0.7 nmole/ml·min for nontumor regions compares well with previously published data on both humans and animals (*19,32,39,40*). The tumor to nontumor ratio was 1.7 on average. This contrast is quite sufficient for tumor detection. Furthermore, considering the heterogeneity of the tumors, the results obtained so far indicate that a high specificity and selectivity of TYR-PET can be expected. The nontumor PSR values found should not be interpreted as typical however, as the PSR values in the contralateral hemisphere may be affected by the presence of the tumor and by the therapeutic strategies employed, such as radiotherapy.

Correction of the plasma activity values for the presence of metabolites is essential. Especially the $^{11}CO_2$ level becomes significant within 5 min and remains so during the rest of the study. The expiration of $^{11}CO_2$ is not able to

TABLE 2
Protein Synthesis Rates in Humans

Subject no.	Dose (MBq)	PSR Tumor (nmole/ml·min)	PSR Control (nmole/ml·min)	Ratio	Histology
1	396	2.05	1.64	1.25	Lipidized glioblastoma
2	137	0.15	0.12	1.25	Low-grade astrocytoma
3	126	*	0.38	—	—
4	189	0.68	0.49	1.39	Metastasis/gliobastoma
5	93	1.64	0.67	2.45	Glioblastoma
6	222	0.98	0.66	1.47	Astrocytoma
7	403	—	0.82	—	Meningioma
8	229	1.76	0.95	1.85	Oligodendroglioma
9	377	1.08	0.47	2.27	Malignant astrocytoma
10	370	0.89	0.44	2.02	Oligodendroglioma
11	377	0.97	0.62	1.56	Necrotic tissue and inflammatory cells
mean ± s.d.	265 ± 115	1.13 ± 0.59	0.66 ± 0.39	1.72 ± 0.44	

*No increased uptake observed.

keep the plasma radioactivity values at negligible levels in accordance with previous observations (*41*). Labeled plasma proteins were negligible for the first 20 min only. Of the acid-soluble metabolites only ^{11}C-L-DOPA reached significant levels (≤8%) which appeared 10 min postinjection. The detection of L-DOPA by HPLC enabled us to establish only a single value per study. Because HPLC of multiple samples will remain impractical, we must resort to a normalized or standardized curve established over many subjects. The data presented here show consistency which indicates that this option is actually feasible.

The graphical Patlak analysis further enhances these methods as it has a robustness against metabolites. The relation between the measured total plasma radioactivity, C_t^*, including the plasma metabolite radioactivity, and the free plasma tyrosine radioactivity can be written as $C_p^* = (1 - \alpha)\, C_t^*$, where α is the metabolite fraction. Ignoring the plasma metabolites is equivalent to substituting C_t^* for C_p^* in equation 14. However, the integral $\int C_t^*(\tau)\, d\tau$ is determined mainly by the initial data when overall plasma radioactivity is high and the metabolite fraction is still low i.e. $\int C_t^*(\tau)\, d\tau \approx \int C_p^*(\tau)\, d\tau$. Now, the slope between the distribution volume (C_i^*/C_p^*) and the apparent time ($\int C_p^*(\tau)d\tau/C_p^*(t)$) relates to the PSR as (Eq. 9 and 14):

$$\frac{PSR}{C_p} = \frac{(C_i^*/C_t^*)_{t2} - (C_i^*/C_t^*)_{t1}}{(\int C_t^*\, d\tau/C_t^*)_{t2} - (\int C_t^*\, d\tau/C_t^*)_{t1}}$$

$$\approx \frac{(C_i^*/\beta C_p^*)_{t2} - (C_i^*/\beta C_p^*)_{t1}}{(\int C_p^*\, d\tau/\beta C_p^*)_{t2} - (\int C_p^*\, d\tau/\beta C_p^*)_{t1}} \qquad \text{Eq. 17}$$

with $\beta = 1/(1 - \alpha)$.

Therefore, in the instance that the metabolite fraction is approximately constant ($\beta_{t1} \approx \beta_{t2}$), it can be divided out of Equation 17, indicating that the PSR thus calculated is not affected by constant plasma metabolite fractions. Combined with the relatively low ^{11}C-L-DOPA activity (<7%) this effect may explain why the observed Patlak curves are easily fitted with a straight line even though the ^{11}C-L-DOPA activity was not corrected for. Considering the values for the remaining tyrosine activity in plasma (Table 1), which shows a rather low variation, one could also consider a modeling approach for the metabolite fraction which requires only a limited number of samples (*42*).

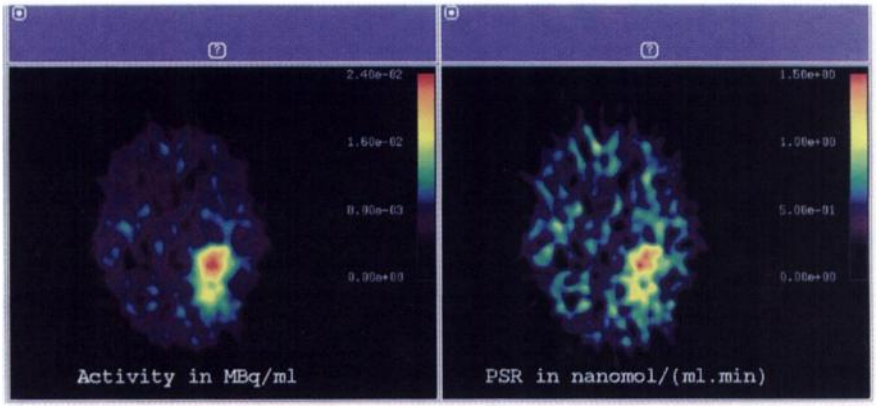

FIGURE 6. Activity and parametric images of a subject with a malignant astrocytoma in the parieto occipital region. The parametric image is obtained by calculating the PSR value on a pixel by pixel basis as described in the text.

Transport of amino acids by the erythrocytes is well established (*43–49*) and this explains the differences in the measured plasma activity as a function of measurement time, in other words, the measured apparent plasma activity depends on the time it takes to separate plasma and erythrocytes. This represents a problem as free plasma ^{11}C-TYR cannot be determined by simple centrifugation of a blood sample and measurement of plasma radioactivity. This may very well explain why our kinetic model fits showed so many problems. Infusion of the tracer over a longer period, cooling of the plasma samples to freezing temperatures or deconvolution of the time activity data could possibly reduce these problems. In the mean time the results of kinetic modeling and curve fitting should be interpreted with caution. Fortunately, it can be shown (see appendix) that the Patlak method is hardly affected by the exchange of ^{11}C-TYR between plasma and erythrocytes. Although the efficacy of this Patlak analysis does not prove the model, it does support it strongly. We conclude that the presented model is adequate for the determination of the PSR and that the presented problems must mainly be attributed to the dynamic exchange of ^{11}C-TYR between plasma and erythrocytes.

Recently, it was shown (*50*) that the accumulation of the labeled amino acids (L-[methyl-^{3}H]methionine, and L-2-[^{18}F]fluorotyrosine) represent amino acid transport whereas L-[1-^{14}C]leucine represents the protein synthesis rate. This indicates that only in vivo uptake of carboxyl labeled amino acids, such as L-[1-^{11}C]leucine and L-[1-^{11}C]tyrosine, is representative of PSR. Noncarboxyl labeled amino acids may still be of some clinical value in tumor detection, as they appear to be reliable markers of tumor tissue. However, for tumor identification patient follow-up or therapy evaluation, a quantitative analysis such as the PSR, appears to be essential. Furthermore, although the radiochemistry of methyl labeled amino acids (*8*) is considered to be relatively simple as compared to the synthesis of carboxyl labeled amino acids, preliminary data on a new synthesis strategy for ^{11}C-TYR, to be published separately, indicate that a fast and simple synthesis is feasible which should facilitate the use of carboxyl labeled amino acids in clinical settings. Finally, tissue metabolite activities of 2–3% for ^{11}C-TYR compare favorably with similar studies using L-[methyl-^{11}C]methionine or L[1-^{11}C]methionine showing metabolite activity values of 10–17% (*17*). Apparently, this relates to the different metabolic pathways for tyrosine and methionine. Thus the application of ^{11}C-TYR and L-[1-^{11}C]leucine is considered to be superior to the other labeled amino acids mentioned.

A final problem concerns the discrepancy between endogenous and exogenous amino acid concentrations. In particular, the recycling of amino acids from proteins (*13,25,34,35*) indicates that the PSR is not a measure of the net unlabeled protein synthesis as shown in the model section. Therefore, it is important to emphasize that the PSR should be understood as the amino acid incorporation rate. Because the transport of amino acids between plasma and precursor pool is faster than the amino acid incorporation rate ($k_1, k_2 \gg k_3$) the effect of recycling on the amino acid incorporation rate can be neglected ($\varepsilon = 1$ in Eq. 8). Consequently, even in the instance that the rate constant obtained with L-[1-^{11}C]leucine used to estimate ε, is not applicable for ^{11}C-TYR or that the recycling differs between tumor and normal tissue, or even between various tissues, this would still have little effect on the calculated amino acid incorporation rates.

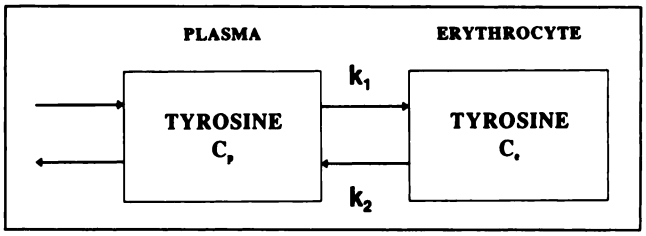

FIGURE 7. Model describing the dynamic exchange of tyrosine between plasma and erythrocyte compartments.

CONCLUSION

The amino acid incorporation rate, generally described as protein synthesis rate (PSR), can be assessed using carboxylic labeled amino-acids such as ^{11}C-TYR. In animals labeled tissue metabolites are below 4% of total tissue radioactivity and are therefore neglected in the model. Labeled plasma metabolites, on the other hand, rise continuously to 50% of total plasma radioactivity at 40 min. After correction of the total plasma radioactivity for the metabolite fraction, a Patlak analysis may be performed to calculate the PSR. Using the Patlak analysis an average non-tumor brain PSR of 0.7 nmole/ml·min was found while the tumor to non-tumor ratio was 1.7 on average. The determination of the labeled plasma metabolites is laborious. However, only the determination of ^{11}C-L-DOPA plasma levels by HPLC requires special attention, whereas the determination of $^{11}CO_2$ and labeled protein in plasma using the method presented here is simple to implement. The PSR values reported here were obtained without correction for plasma ^{11}C-L-DOPA levels. Apparently, this correction is relatively minor and can be neglected. Therefore it is concluded that the application of TYR-PET in a clinical setting is possible.

APPENDIX

Whole blood is modeled as a two-compartment model (Fig. 7). Tyrosine within the erythrocyte can only interact with the plasma compartment. The plasma compartment also interacts with a unknown number of other tissue compartments. A whole blood sample shows identical tyrosine concentrations in both compartments after a few minutes of storage at room temperature, indicating equilibrium. This average activity (C_t^*) is given by:

$$C_t^* = \frac{V_p C_p^* + V_e C_e^*}{V_p + V_e}, \qquad \text{Eq. A1}$$

with C_p^* and C_e^* the plasma and erythrocyte activity at the time of sampling, and V_p and V_e the respective volumes.

From the model the transfer function can easily be deduced to be:

$$H(s) = \frac{C_e^*(s)}{C_p^*(s)} = \frac{k_1}{k_2} \frac{1}{s/k_2 + 1}. \qquad \text{Eq. A2}$$

This describes a low-pass filter with gain k_1/k_2 and cutoff frequency k_2. The data show that the activity concentrations in the plasma and in the erythrocyte compartments are identical after a certain time (T), showing that the gain of the transfer function must be 1 and thus $k_1 = k_2 = k$. For $t > T$ it also follows that $C_e^* \cong C_p^*$ and thus $C_t^* \cong C_p^*$.

From the final value theorem for Laplace transforms, it can be shown that for a filter written as:

$$H(s) = \frac{1 + a_1 s^1 + a_2 s^2 + a_n s^n}{1 + b_1 s^1 + b_2 s^2 + b_m s^m}, \qquad \text{Eq. A3}$$

such as the filter in equation A2, the following equation holds

$$\int_0^\infty h(t) \otimes C_p^*(t)\, dt = \int_0^\infty C_p^*(t)\, dt. \qquad \text{Eq. A4}$$

Thus

$$\int_0^\infty C_t^*(t)\, dt = \frac{V_p}{V_p + V_e} \int_0^\infty C_p^*(t)\, dt$$

$$+ \frac{V_e}{V_p + V_e} \int_0^\infty h(t) \otimes C_p^*(t)\, dt = \frac{V_p}{V_p + V_e} \int_0^\infty C_p^*(t)\, dt$$

$$+ \frac{V_e}{V_p + V_e} \int_0^\infty C_p^*(t)\, dt = \int_0^\infty C_p^*(t)\, dt. \qquad \text{Eq. A5}$$

Strictly speaking, the above is true only for $t \to \infty$. However, considering the dynamics of tyrosine in blood, it can safely be assumed for $t > T$. In conclusion, we find that for $t > T$ $C_t^*(t) \cong C_p^*(t)$ as well as $\int C_t^*(\tau)\, d\tau = \int C_p^*(\tau)\, d\tau$. Because a graphical Patlak-Gjedde analysis uses only the data for $t > T$, it should give the correct result whereas a least squares model fit will not.

ACKNOWLEDGMENTS

The authors thank Dr. J. van den Hoff, Department of Nuclear Medicine, University Hospital Hannover, Hannover, Germany, for his support in developing the program for PSR calculations on a pixel-by-pixel basis.

REFERENCES

1. Ishiwata K, Takahashi T, Iwata R, et al. Tumor diagnosis by PET: potential of seven tracers examined in five experimental tumors including an artificial metastasis model. *Nucl Med Biol* 1992;19:611–618.
2. Hawkins RA, Phelps ME, Huang SC. Effects of temporal sampling, glucose metabolic rates and disruptions of the blood-brain barrier on the FDG model with and without a vascular compartment: studies in human brain tumors with PET. *J Cereb Blood Flow Metab* 1986;6:170–183.
3. Di Chiro G. Positron emission tomography using [^{18}F]fluorodeoxyglucose in brain tumors, a powerful diagnostic and prognostic tool. *Invest Radiol* 1987;22:360–371.
4. Ericson K, Lilja A, Bergstrom M, et al. Positron emission tomography with ([^{11}C]methyl)-L-methionine, [^{11}C]D-glucose, and [^{68}Ga]EDTA in supratentorial tumors. *J Comput Assist Tomogr* 1985;9:683–689.
5. Sasaki M, Ichiya Y, Kuwabara Y. Ringlike uptake of [^{18}F]FDG in brain abscess: a PET study. *J Comput Assist Tomogr* 1990;14:486–487.
6. Kubota R, Yamada S, Kubota K, Ishiwata K, Tamahashi N, Ido T. Intratumoral distribution of fluorine-18-fluorodeoxyglucose in vivo: high accumulation in macrophages and granulation tissues studied by microautoradiography. *J Nucl Med* 1992;33:1972–1980.
7. Wahl RL, Fisher SJ. A comparison of FDG, L-methionine and thymidine accumulation into experimental infections and reactive lymph nodes. *J Nucl Med* 1993;34:104P.
8. Vaalburg W, Coenen HH, Crouzel C, et al. Amino acids for the measurement of protein synthesis in vivo by PET. *Nucl Med Biol* 1992;19:227–237.
9. Phelps ME, Barrio JR, Huang SC, Keen RE, Chugani H, Mazziotta JC. Criteria for the tracer kinetic measurement of cerebral protein synthesis in humans with positron emission tomography. *Ann Neurol* 1984;15 (suppl): S192–S202.
10. Lilja A, Lundquist H, Olsson Y. Positron emission tomography and computed tomography in differential diagnosis between recurrent or residual glioma and treatment-induced brain lesions. *Acta Radiol* 1989;30:121–128.
11. Fujiwara T, Matsuzawa T, Kubota K, et al. Relationship between histologic type of primary lung cancer and carbon-11-L-methionine uptake with positron emission tomography. *J Nucl Med* 1989;30:33–37.
12. Ishiwata K, Ido T, Abe Y. Tumor uptake studies of S-adenosyl-L-[methyl-^{11}C]methionine and L-[methyl-^{11}C]methionine. *Nucl Med Biol* 1988;15:123–126.
13. Planas AM, Prenant C, Mazoyer BM, Comar D, Di Giamberardino L. Regional cerebral L-[^{14}C-methyl]methionine incorporation into proteins: evidence for methionine recycling in the rat brain. *J Cereb Blood Flow Metab* 1992;12:603–612.
14. Daemen BJ, Zwertbroek R, Elsinga PH, Paans AM, Doorenbos H, Vaalburg W. PET studies with L-[1-^{11}C]tyrosine, L-[methyl-^{11}C]methionine and ^{18}F-fluorodeoxyglucose in prolactinomas in relation to bromocryptine treatment. *Eur J Nucl Med* 1991;18:453–460.
15. Lindholm P, Leskinen-Kallio S, Minn H, et al. Comparison of fluorine-18-fluorodeoxyglucose and carbon-11-methionine in head and neck cancer. *J Nucl Med* 1993;34:1711–1716.
16. Bolster JM, Vaalburg W, Elsinga PH, Ishiwata K, Vissering H, Woldring MG. The preparation of ^{11}C-carboxylic labeled L-methionine for measuring protein synthesis. *J Label Compd Radiopharm* 1986;23:1081–1082.
17. Ishiwata K, Vaalburg W, Elsinga PH, Paans AM, Woldring MG. Comparison of L-[1-^{11}C]methionine and L-methyl-[^{11}C]methionine for measuring in vivo protein synthesis rates with PET. *J Nucl Med* 1988;29:1419–1427.
18. Keen RE, Barrio JR, Huang SC, Hawkins RA, Phelps ME. In vivo cerebral protein synthesis rates with leucyl-transfer RNA used as a precursor pool: determination of biochemical parameters to structure tracer kinetic models for positron emission tomography. *J Cereb Blood Flow Metab* 1989;9:429–445.
19. Hawkins RA, Huang SC, Barrio JR, et al. Estimation of local cerebral protein synthesis rates with 1-[^{11}C]leucine and PET: methods, model and results in animal and humans. *J Cereb Blood Flow Metab* 1989;9:446–460.
20. Barrio JR, Keen RE, Ropchan JR, et al. L-[1-^{11}C]leucine: routine synthesis by enzymatic resolution. *J Nucl Med* 1983;24:515–521.
21. Luurtsema G, Medema J, Elsinga PH, Visser GM, Vaalburg W. Robotic synthesis of L-[1-^{11}C]tyrosine. *Appl Radiat Isot* 1994;45:821–828.
22. Halldin C, Schoeps KO, Stone-Elander S, Wiesel FA. The Bücherer-Strecker synthesis of D- and L-(1-^{11}C)tyrosine and the in vivo study of L-(1-^{11}C)tyrosine in human brain using positron emission tomography. *Eur J Nucl Med* 1987;13:288–291.
23. Daemen BJ, Elsinga PH, Paans AMJ, Wieringa AR, Konings ATW, Vaalburg W. Radiation-induced inhibition of tumor growth as monitored by PET using L-[1-^{11}C]tyrosine and fluorine-18-fluorodeoxyglucose. *J Nucl Med* 1992;33:373–379.
24. Go KG, Prenen GH, Paans AM, Vaalburg W, Kamman RL, Korf J. Positron emission tomography study of ^{11}C-acetoacetate uptake in a freezing lesion in cat brain, as correlated with ^{11}C-tyrosine and 18F-fluorodeoxyglucose uptake, and with proton magnetic resonance imaging. *Adv Neurol* 1990;52:525–528.
25. Mitsuka S, Diksic M, Takada A, Yamamoto YL. Influence of the tumor mass on the valine rate constants and on valine incorporation into proteins in an experimental brain tumor model. *Neurochem Int* 1992;20:537–551.
26. Kirikae M, Diksic M, Yamamoto YL. Quantitative measurements of regional glucose utilization and rate of valine incorporation into proteins by double-tracer autoradiography in the rat brain tumor model. *J Cereb Blood Flow Metab* 1989;9:87–95.
27. Coenen HH, Kling P, Stöcklin G. Cerebral metabolism of L-[2-

[18F]fluorotyrosine a new PET tracer of protein synthesis. *J Nucl Med* 1989;30:1367–1372.
28. Wienhard K, Herholz K, Coenen HH, et al. Increased amino acid transport into brain tumors measured by PET of L-(2-[18F]fluorotyrosine. *J Nucl Med* 1991;32:1338–1346.
29. Bodsch W, Coenen HH, Stöcklin G, Takahashi K, Hossmann KA. Biochemical and autoradiographic study of cerebral protein synthesis with [18F] and [14C]fluorophenylalanine. *J Neurochem* 1988;50:979–983.
30. Van Langevelde A, Van der Molen HD, Journee-de Korver JG, Paans AM, Pauwels EK, Vaalburg W. Potential radiopharmaceuticals for the detection of ocular melanoma: Part III. A study with 14C-and 11C-labelled tyrosine and dihydroxyphenylalanine. *Eur J Nucl Med* 1988;14:382–387.
31. Ishiwata K, Vaalburg W, Elsinga PH, Paans AMJ, Woldring MG. Metabolic studies with 1-[1-14C]tyrosine for the investigation of a kinetic model to measure protein synthesis rates with PET. *J Nucl Med* 1988;29:524–529.
32. Paans AM, Elsinga PH, Vaalburg W. Carbon-11-labeled tyrosine as a probe for modelling the protein synthesis rate. In: Mazoyer BM, Heiss WD, Comar D, eds. *PET studies on amino acid metabolism and protein synthesis*. Dordrecht, The Netherlands: Kluwer Academic; 1993:161–174.
33. Fox KAA, Abendschein DR, Ambos HD, Sobel BE, Bergmann SR. Efflux of metabolized and nonmetabolized fatty acid from canine myocardium: implications for quantifying myocardial metabolism tomographically. *Circ Res* 1985;57:232–243.
34. Smith CB, Deibler GE, Eng N, Schmidt K, Sokoloff L. Measurement of local cerebral protein synthesis in vivo: influence of recycling of amino acids derived from protein degradation. *Proc Natl Acad Sci USA* 1988;85:9341–9345.
35. Widmann R, Kocher M, Ernestus RI, Hossmann KA. Biochemical and autoradiographical determination of protein synthesis in experimental brain tumors of rats. *J Neurochem* 1992;59:18–25.
36. Phelps ME, Huang SC, Hoffman EJ, Selin CE, Sokoloff L, Kuhl DE. Tomographic measurement of local cerebral glucose metabolic rate in humans with (F-18)2-fluoro-2-deoxyglucose: validation of method. *Ann Neurol* 1979;6:371–388.
37. Patlak CS, Blasberg RG, Fenstermacher JD. Graphical evaluation of blood-to-brain transfer constants from multiple-time uptake data. *J Cereb Blood Flow Metab* 1983;3:1–7.
38. Patlak CS, Blasberg RG. Graphical evaluation of blood-to-brain transfer constants from multiple-time uptake data: generalizations. *J Cereb Blood Flow Metab* 1985;5:584–590.
39. Ericson K, Blomquist G, Bergström M, Eriksson L, Stone-Elander S. Application of a kinetic model on the methionine accumulation in intracranial tumours studied with positron emission tomography. *Acta Radiol* 1987; 28:505–509.
40. O'Tuama LA, Guilarte TR, Douglass KH, et al. Assessment of [11C]-L-methionine transport into the human brain. *J Cereb Blood Flow Metab* 1988;8:341–345.
41. Shields AF, Graham MM, Kozawa SM, et al. Contribution of labeled carbon dioxide to PET imaging of carbon-11-labeled compounds. *J Nucl Med* 1992;33:581–584.
42. Huang SC, Barrio JR, Yu DC, et al. Modelling approach for separating blood time-activity curves in positron emission tomographic studies. *Phys Med Biol* 1991;36:749–761.
43. Hagenfeldt L, Arvidsson A. The distribution of amino acids between plasma and erythrocytes. *Clin Chim Acta* 1980;100:133–141.
44. Heitmann RN, Bergman EN. Transport of amino acids in whole blood and plasma of sheep. *Am J Physiol* 1980;239:E242–E247.
45. Widmer J, Gaillard JM, Tissot R. L-tyrosine and L-tryptophan transport in red blood cells in normal subjects. Effects of other amino acids, temperature and medium of incubation. *Neuropsychobiology* 1986;15:7–12.
46. Young JD, Jones SE, Ellory JC. Amino acid transport via the red cell anion transport system. *Biochim Biophys Acta* 1981;645:157–160.
47. Young JD, Jones SE, Ellory JC. Amino acid transport in human and in sheep erythrocytes. *Proc R Soc Lond [Biol]* 1980;209:355–375.
48. Harvey CM, Ellory JC. Identification of amino acid transporters in the red blood cell. *Methods Enzymol* 1989;173:122–160.
49. Rosenberg R. Amino acid transport in human red blood cells. *Acta Psychiatr Scand Suppl* 1988;345:25–28.
50. Ishiwata K, Kubota K, Murakami M, et al. Re-evaluation of amino acid PET studies: can the protein synthesis rates in brain and tumor tissues be measured in vivo? *J Nucl Med* 1993;34:1936–1943.